Materials Science Forum vols. 143-147 (1994) pp. 815-820

NONLINEAR ZEEMAN SPLITTING AND ELECTRON-PHONON COUPLING

J. SCHÖPP[a], R. HEITZ[b], A. HOFFMANN[b] and U. SCHERZ[a]

[a]Institut für Theoretische Physik and [b]Institut für Festkörperphysik
Technische Universität Berlin, Hardenbergstr. 36, 10623 Berlin, Germany

Keywords: Transition-metal impurity, Jahn-Teller effect, Zeeman effect, CdS, Ni.

Abstract

A calculation of the observed $^3T_1(F)$ ground state and $^3T_1(P)$ excited state fine structure of the CdS:Ni^{2+} center using an intermediate coupling to a T_2 local vibrational mode is presented. For the first time such a fit is confirmed by the good agreement between the parameter-free calculation of the Zeeman behaviour and the isotope shifts with experimental data.

1. Introduction

Early investigations of transition-metal ions in II-VI compounds were done by Weakliem [1], who explained the observed fine structure within the framework of static crystal-field theory. But the continuous development and refinement of experimental techniques and instrumentation lead to a variety of new observed data which can not be explained by this model. One prominent example for the need of more refined models is CdS:Ni^{2+}, which was intensively studied by Broser et al. [2]. Using the static model, it was impossible to explain e.g. the isotope shifts or the fine structure of several optical transitions. Because transition-metal ions in semiconductors are well known to show a Jahn-Teller effect, Nestler et al. [3] introduced the concept of an intermediate electron-phonon coupling, which allowed them to explain the fine structure of the $^3T_1(F)$ and $^3T_1(P)$ multiplets and the isotope shifts of the first four excited $^3T_1(P)$ levels. But they were not able to describe the Zeeman behaviour and there were not enough experimental data to do an unambiguous fit of the crystal-field parameters. In the meantime, further magneto-optical measurements with high power lasers lead to a variety of new data, which were, supplementary to the availability of powerful supercomputers, the starting point for new theoretical investigations. Here, we demonstrate that the observation of six energy differences for both of the $^3T_1(F)$ and $^3T_1(P)$ multiplets leads to an unambiguous fit of the parameters, with which the isotope effect and the Zeeman behaviour of the system can be understood.

2. Fine structure

With the development of high-power lasers new d-d luminescence lines and bands in semiconductors could be detected. A comparison of the resulting emission spectra with the corresponding absorptions often yields a manifold of d-d transitions which can be understood only in terms of a Jahn-Teller effect. A typical example is the emission (lower curve of figure 1) and transmission (upper curve) spectrum of a Ni-doped CdS crystal in the spectral region between 1.38 and 1.56 eV. The insert shows the different observed absorption and luminescence Ni^{2+} transitions of the energy level scheme. The emission spectrum represents the Ni^{2+} fine-structure splittings of the $^3T_1(F)$ ground state, while the absorption spectrum reproduces the splittings of the excited states. The emission lines O_1, E_1 and E_4 are transitions from the ground state of the $^3T_1(P)$ term to different ground and excited states of the $^3T_1(F)$ term. The energy distances between the O_1, E_1 and E_4 lines are only understandable in terms of an electron-phonon coupling in the ground-state multiplet. Similar effects occur for the splittings of the excited states which can be derived from the absorption spectrum.

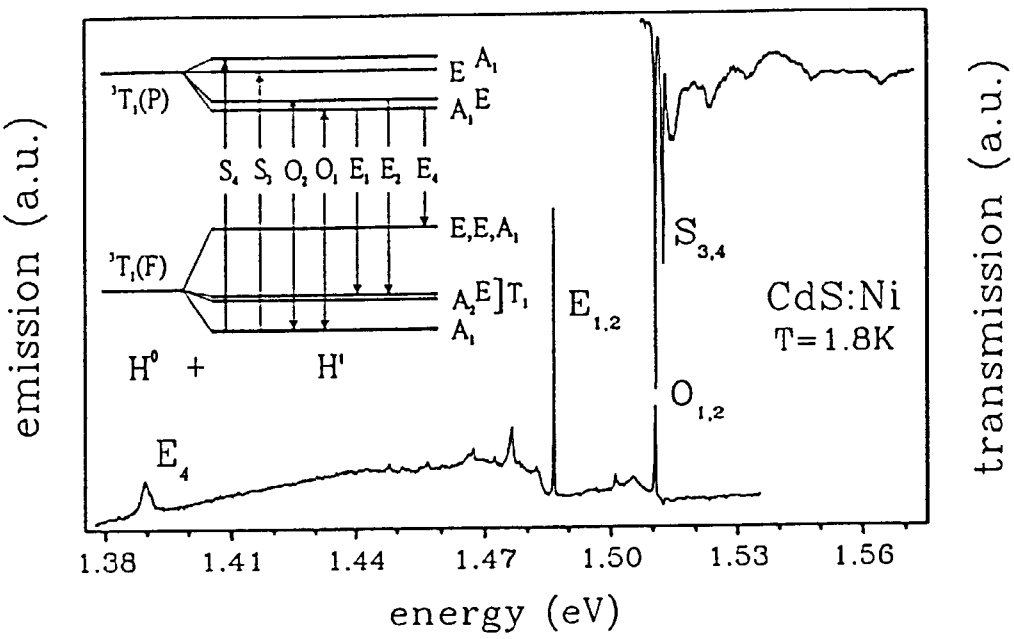

Figure 1: Transmission and emission spectrum of the $^3T_1(F) \leftrightarrow {}^3T_1(P)$ Ni^{2+} transitions in CdS. The insert shows the corresponding energy-level scheme and H' denotes the fine-structure operator in C_{3v} symmetry.

The fit of the observed fine structures in a dynamical model, which include the Jahn–Teller interaction, is not always unambiguous. Further information about the system is obtained by the evaluation of an isotope effect in the spectra. In order to describe the isotope shift, we introduce the concept of different local vibrational modes coupling to the initial and final electronic states, both having T_2 symmetry but different energies. This is because only T_2 modes can move the central ion and therefore can cause an isotope shift. Taking into account spin–orbit coupling and the trigonal deviation from tetrahedral symmetry, we use the following Hamiltonian in the framework of the adiabatic approximation:
$H_{tot} = E_{el} + H_{ph} + H_{JT} + H_{C_{3v}} + H_{so}$. E_{el} is the electronic energy and $H_{ph}, H_{JT}, H_{C_{3v}}, H_{so}$ denote the operators of phonons, Jahn–Teller effect, trigonal field and spin–orbit coupling. The energies of the resulting eigenvalue problem depend on four parameters corresponding to the perturbation operators: $\hbar\omega$: phonon-energy of local mode, E_{JT}: Jahn–Teller energy, k: trigonal crystal–field parameter, λ: spin–orbit coupling parameter. These parameters were fitted independently for the $^3T_1(F)$ and $^3T_1(P)$ multiplets by means of an evolution strategy. Due to the variety of experimental data we were able to determine unambiguously the fine–structure parameters by fitting six energy differences to the observed values. We use up to ten excited states of the local vibrational mode. By increasing the number of phonons from three to ten it is seen that we have to take into account at least eight phonons to achieve convergence. Comparing the calculated and observed energy differences (table 1), we obtain for both multiplets good agreement between experiment and theory.

$^3T_1(F)$						
	E	A_2	E	E	E	E
Observed	178.2	189.7	194.7	227.0	276.0	974.1
Calculated	177.9	189.7	194.7	233.0	275.0	974.1
$^3T_1(P)$						
	E	E	A_1	E	E	A_1
Observed	1.3	12.5	15.5	27.3	57.3	212.0
Calculated	1.3	12.5	15.5	27.8	55.9	210.5

Table 1: Comparison between observed and calculated energies for the $^3T_1(F)$ and $^3T_1(P)$ multiplet. The energy levels are denoted corresponding to their symmetry. The table contains energy differences in cm^{-1} relative to the respective ground state.

The corresponding parameters have reasonable values: The spin–orbit coupling parameter of the ${}^3T_1(P)$ term, $\lambda_P = -225$ cm^{-1}, is close to that of Weakliem [1] $\lambda = -250$ cm^{-1}. From static–crystal field theory it is known that the ratio of the spin–orbit coupling parameters of the ${}^3T_1(F)$ and ${}^3T_1(P)$ terms is -1.5, which is near to our value of -1.6. The k parameters are small in both cases ($k_F = 12$ cm^{-1}, $k_P = 12$ cm^{-1}), which demonstrates the weakness of the trigonal crystal field. The Huang–Rhys factors S are equal in both cases and are close to one. This verifies our assumption of an intermediate Jahn–Teller coupling. The phonon energies ($\hbar\omega_F = 170$ cm^{-1}, $\hbar\omega_P = 315$ cm^{-1}) agree well with Raman-detected local vibrational modes ($\hbar\omega = 185$ cm^{-1} and $\hbar\omega = 310$ cm^{-1}).

3. Isotope effect

The calculation of the isotope shift gives us an important tool to check the fine–structure fit. Assuming that the main contribution to the mass dependence of a particular level comes from the coupling to a single local vibrational mode, the change of energy level E_ν with mass M is obtained by [4]:

$$\frac{dE_\nu}{dM} = \frac{\partial E_\nu}{\partial(\hbar\omega_\nu)} \frac{\partial(\hbar\omega_\nu)}{\partial M} . \tag{1}$$

The first factor is calculated by exploiting the fine–structure results, leading to the values of 1.15, 1.14, 1.14, and 1.32 for the first four excited levels of the ${}^3T_1(P)$ term. The second factor is obtained by calculating the dynamical matrix of a cluster of 159 atoms, built up of 12 coordination shells around the defect. The potential energy is a sum of Coulomb and elastical energy, where the elastical part is described by the valence–force model of Keating [5].

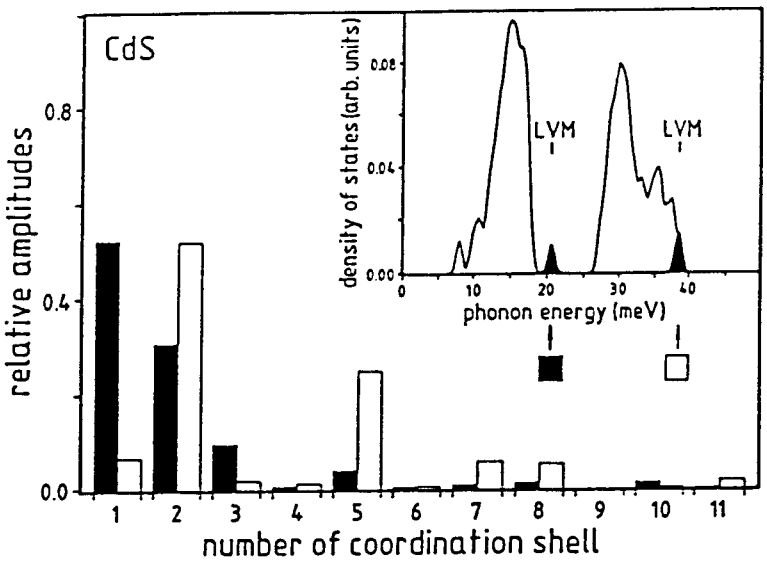

Figure 2: Contribution of each shell to the total vibration for the two local modes. The bars indicate the contribution of the eigenvector of the dynamical matrix with respect to the atoms in a particular coordination shell. The insert shows the density of phonon states of a cluster of 159 vibrating atoms with the Ni atom at the center.

The explanation of the isotope shift is strongly correlated with the existence of local vibrational modes moving the defect. Looking at figure 2 we see, that these conditions are fulfilled: the first two shells (defect and four nearest neighbours) contain large vibration amplitudes for both modes with energies $\hbar\omega = 170$ cm^{-1} ($\hbar\omega = 315$ cm^{-1}), coupled to the ${}^3T_1(F)$ (${}^3T_1(P)$) term. The density of phonon states (insert in figure 2) shows, that these modes lie in the band gap and little above the optical band respectively. Because of the much stronger vibration of the defect in case of the gap mode, we obtain a stronger mass dependence of this mode compared to the mode above the optical band: $\frac{\partial(\hbar\omega)}{\partial M} = -0.73$ cm^{-1} per nucleon mass for $\hbar\omega = 170$ cm^{-1} and $\frac{\partial(\hbar\omega)}{\partial M} = -0.43$ cm^{-1} per nucleon mass for $\hbar\omega = 315$ cm^{-1}. Using equation 1 and the fine–structure results, we obtain the isotope shift. Subtracting the isotope shift of the ground state from the isotope shift of the first four excited level of the ${}^3T_1(P)$ term, we get the energy shift per nucleon mass for the lines O_1, O_2, S_3, S_4, given in table 2.

	O_1	O_2	S_3	S_4
Observed	0.177	0.177	0.161	0.169
Calculated	0.219	0.223	0.223	0.149
Relative Deviation [%]	+23.7	+26.0	+38.5	-12.1

Table 2: Comparison between observed and calculated isotope shifts per nucleon of the transitions O_1, O_2, S_3, S_4. Energies are in cm^{-1}.

The results show a good agreement between observed and calculated isotope shifts. The calculated isotope shift of the transition S_4 is not far from those of the other three shifts, which is at first glance surprising. Ignoring for the moment electron–phonon coupling, the final state of S_4 is in our model a one phonon state, having a vibrational energy of $5/2\ \hbar\omega$ which has to be compared with $3/2\ \hbar\omega$ of the first three excited states having zero phonon character. This would result in different isotope shifts for zero and one phonon states, which are not observed. But taking electron–phonon coupling into account, all four excited states become a mixture of multiphonon states having similar isotope shifts.

4. Zeeman effect

A strong test for the reliability of the fine–structure fit is the calculation of the Zeeman behaviour. The Zeeman effect is computed by adding the Zeeman operator to the total Hamiltonian H_{tot} and solving the corresponding eigenvalue problem with the parameters of the zero–field fit. From the vibronic wavefunctions we performed a parameter–free calculation of the nonlinear Zeeman pattern for magnetic fields parallel and perpendicular to the c-axis (symmetry C_3 and C_s) for the fine–structure lines O_1, O_2, S_3, S_4 (top) and the energy levels E and A_2 of T_1-$^3T_1(F)$ (bottom of figure 3).

Comparing this with experiment (left hand side of figure 3), we see the following: 1. The splitting and the nonlinear behaviour of the O lines is well explained in both symmetries. 2. The calculations of the S lines show in C_s symmetry a repulsion between the S_4 line and one component of the S_3 line, which is a consequence of the no–crossing rule. Looking at the experimental data, we see only two S lines in C_s symmetry, leaving one transition undetected. Considering the S lines in C_3 symmetry, we see a discrepancy: Measurements show a linear splitting of the twofold degenerate level, whereas the calculated behaviour is nonlinear. But the calculated behaviour is easily explained by the repulsion of a nearby level, having the same symmetry. This discrepancy between experiment and theory is unexplained to date. 3. The linear splitting of the E level of T_1-$^3T_1(F)$ in C_s symmetry, to be seen in experiment and in calculation, is explained by the absence of a nearby level of the same symmetry. In C_3 symmetry the calculations show the expected nonlinear splitting of the twofold level, whereas one line is not observed as yet. 4. Considering the zero–phonon level A_2 of T_1-$^3T_1(F)$ (190 cm^{-1} above the ground state) in C_s symmetry, we see agreement between computed and observed behaviour for small magnetic fields. The positive slope of the curve in C_3 symmetry, seen in experiment and calculation, is explained by the existence of a nearby state with the same symmetry lying below the A_2 level. Looking at the phonon energy of the ground state (170 cm^{-1}), it is clear that this state is a multi–phonon level.

Our results demonstrate the close correspondence between the nonlinear Zeeman splitting and the electron–phonon coupling: The correct interpretation of the fine structure is a necessary prerequisite for the understanding of the Zeeman behaviour of such Jahn–Teller systems.

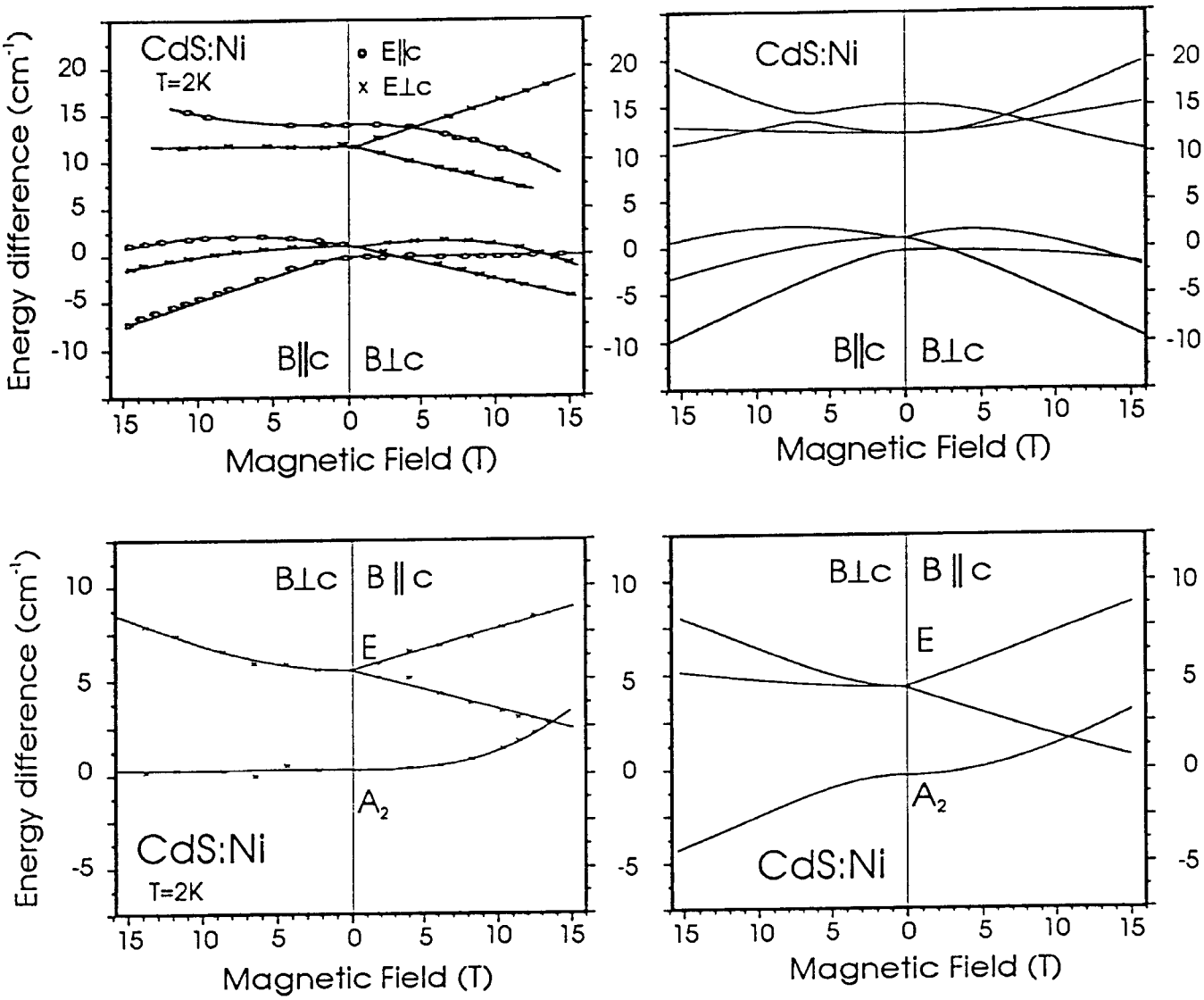

Figure 3: Calculated (right) and observed (left) Zeeman behaviour of the transitions O_1, O_2, S_3 and S_4 (top) and of the energy levels E and A_2 of $T_1 - {}^3T_1(F)$ (bottom).

5. Conclusion

The successful calculations concerning the fine structure, the Zeeman effect, and the isotope effect clearly demonstrate the usefulness of the underlying model, the Jahn–Teller coupling of different T_2 modes in the ground and excited state being its foundation. One important requirement to get reliable results is the convergence and definiteness of the parameters, which was a lack in many earlier investigations. We ensured these demands by using up to 10 phonons and exploiting the variety of experimental data for our fit. For the first time we performed a parameter-free calculation of the Zeeman behaviour, which confirmed the fine-structure fit.

References

[1] Weakliem, H.A.: J. Chem. Phys., 1962, 36, 2117
[2] Broser, I., Hoffmann, A., Germer, R., Broser, R., Birkicht, E.: Phys. Rev B, 1986, 33, 8196
[3] Nestler, B., Hoffmann, A., Xu, L.B., Scherz, U., Broser, I.: J. Phys. C, 1987, 20, 4613
[4] Hoffmann, A., Scherz, U.: J. Crystal Growth, 1990, 101, 385
[5] Keating, P.N.: Phys. Rev., 1966, 145, 637